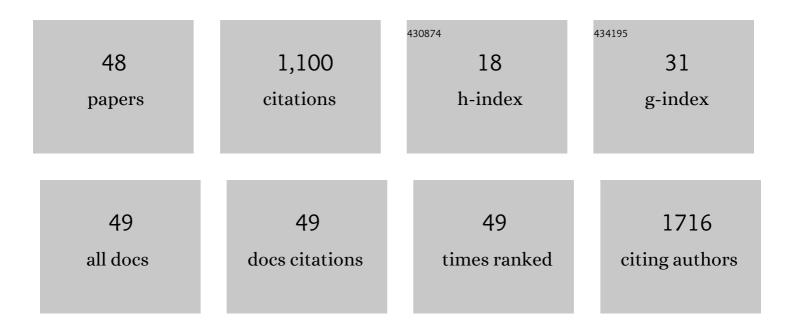
Liang-ping Luo

List of Publications by Year in descending order

Source: https://exaly.com/author-pdf/5895095/publications.pdf Version: 2024-02-01



#	Article	IF	CITATIONS
1	A multifunctional nanotheranostic agent potentiates erlotinib to EGFR wild-type non-small cell lung cancer. Bioactive Materials, 2022, 13, 312-323.	15.6	21
2	MR imaging guided iron-based nanoenzyme for synergistic Ferroptosisâ^'Starvation therapy in triple negative breast cancer. Smart Materials in Medicine, 2022, 3, 159-167.	6.7	8
3	Facile synthesis of near-infrared responsive on-demand oxygen releasing nanoplatform for precise MRI-guided theranostics of hypoxia-induced tumor chemoresistance and metastasis in triple negative breast cancer. Journal of Nanobiotechnology, 2022, 20, 104.	9.1	6
4	Comprehensive Analysis of PDLIM3 Expression Profile, Prognostic Value, and Correlations with Immune Infiltrates in Gastric Cancer. Journal of Immunology Research, 2022, 2022, 1-18.	2.2	1
5	Comparison of percentage changes in quantitative diffusion parameters for assessing pathological complete response to neoadjuvant therapy in locally advanced rectal cancer: a meta-analysis. Abdominal Radiology, 2021, 46, 894-908.	2.1	2
6	Monitoring Treatment Efficacy of Antiangiogenic Therapy Combined With Hypoxia-Activated Prodrugs Online Using Functional MRI. Frontiers in Oncology, 2021, 11, 672047.	2.8	6
7	Perivascular cellâ€derived extracellular vesicles stimulate colorectal cancer revascularization after withdrawal of antiangiogenic drugs. Journal of Extracellular Vesicles, 2021, 10, e12096.	12.2	20
8	NIR-Triggered Blasting Nanovesicles for Targeted Multimodal Image-Guided Synergistic Cancer Photothermal and Chemotherapy. ACS Applied Materials & Interfaces, 2021, 13, 35376-35388.	8.0	17
9	Performing IVIM-DWI using the multifunctional nanosystem for the evaluation of the antitumor microcirculation changes. Magnetic Resonance Materials in Physics, Biology, and Medicine, 2020, 33, 517-526.	2.0	9
10	Evaluating the Treatment Efficacy of Nano-Drug in a Lung Cancer Model Using Advanced Functional Magnetic Resonance Imaging. Frontiers in Oncology, 2020, 10, 563932.	2.8	6
11	DTI-based radiomics signature for the detection of early diabetic kidney damage. Abdominal Radiology, 2020, 45, 2526-2531.	2.1	18
12	Monitoring tumour microenvironment changes during anti-angiogenesis therapy using functional MRI. Angiogenesis, 2019, 22, 457-470.	7.2	43
13	Ginsenoside F1 promotes angiogenesis by activating the IGF-1/IGF1R pathway. Pharmacological Research, 2019, 144, 292-305.	7.1	62
14	Precise delivery of a multifunctional nanosystem for MRI-guided cancer therapy and monitoring of tumor response by functional diffusion-weighted MRI. Journal of Materials Chemistry B, 2019, 7, 2926-2937.	5.8	15
15	CT-based machine learning model to predict the Fuhrman nuclear grade of clear cell renal cell carcinoma. Abdominal Radiology, 2019, 44, 2528-2534.	2.1	54
16	Detection of Hyperacute Reactions of Desacetylvinblastine Monohydrazide in a Xenograft Model Using Intravoxel Incoherent Motion DWI and R2* Mapping. American Journal of Roentgenology, 2019, 212, 717-726.	2.2	11
17	Application of High-Resolution CUBE Sequence in Exploring Stroke Mechanisms of Atherosclerotic Stenosis of Middle Cerebral Artery. Journal of Stroke and Cerebrovascular Diseases, 2019, 28, 156-162.	1.6	12
18	Cerebral Perforating Artery Disease. Clinical Neuroradiology, 2019, 29, 533-541.	1.9	5

LIANG-PING LUO

#	Article	IF	CITATIONS
19	Comparison of T1 Mapping and T1rho Values with Conventional Diffusion-weighted Imaging to Assess Fibrosis in a Rat Model of Unilateral Ureteral Obstruction. Academic Radiology, 2019, 26, 22-29.	2.5	17
20	Diagnostic Values of DCE-MRI and DSC-MRI for Differentiation Between High-grade and Low-grade Gliomas. Academic Radiology, 2018, 25, 338-348.	2.5	35
21	Using IVIM-MRI and R2⎠Mapping to Differentiate Early Stage Liver Fibrosis in a Rat Model of Radiation-Induced Liver Fibrosis. BioMed Research International, 2018, 2018, 1-9.	1.9	13
22	Monitoring the Process of Endostar-Induced Tumor Vascular Normalization by Non-contrast Intravoxel Incoherent Motion Diffusion-Weighted MRI. Frontiers in Oncology, 2018, 8, 524.	2.8	21
23	Comparison of image quality and radiation exposure between conventional imaging and gemstone spectral imaging in abdominal CT examination. British Journal of Radiology, 2018, 91, 20170448.	2.2	9
24	A highly hemocompatible erythrocyte membrane-coated ultrasmall selenium nanosystem for simultaneous cancer radiosensitization and precise antiangiogenesis. Journal of Materials Chemistry B, 2018, 6, 4756-4764.	5.8	56
25	Desacetylvinblastine Monohydrazide Disrupts Tumor Vessels by Promoting VE-cadherin Internalization. Theranostics, 2018, 8, 384-398.	10.0	17
26	Carotid DSA based CFD simulation in assessing the patient with asymptomatic carotid stenosis: a preliminary study. BioMedical Engineering OnLine, 2018, 17, 31.	2.7	20
27	Staging of rat liver fibrosis using monoexponential, stretched exponential and diffusion kurtosis models with diffusion weighted imaging- magnetic resonance. Oncotarget, 2018, 9, 2357-2366.	1.8	8
28	Ultrahigh bâ€values MRI in normal human prostate: Initial research on reproducibility and ageâ€related differences. Journal of Magnetic Resonance Imaging, 2017, 46, 801-812.	3.4	9
29	Development and validation of a predictor of insufficient enhancement during the hepatobiliary phase of Gd-EOB-DTPA-enhanced magnetic resonance imaging. Acta Radiologica, 2017, 58, 1174-1181.	1.1	4
30	Monitoring Tumor Response to Antivascular Therapy Using Non-Contrast Intravoxel Incoherent Motion Diffusion-Weighted MRI. Cancer Research, 2017, 77, 3491-3501.	0.9	49
31	Nucleolin-targeted selenium nanocomposites with enhanced theranostic efficacy to antagonize glioblastoma. Journal of Materials Chemistry B, 2017, 5, 3024-3034.	5.8	20
32	A study of noninvasive fractional flow reserve derived from a simplified method based on coronary computed tomography angiography in suspected coronary artery disease. BioMedical Engineering OnLine, 2017, 16, 43.	2.7	26
33	Pericyte-targeting prodrug overcomes tumor resistance to vascular disrupting agents. Journal of Clinical Investigation, 2017, 127, 3689-3701.	8.2	71
34	Head and Neck Cancer Tumor Segmentation Using Support Vector Machine in Dynamic Contrast-Enhanced MRI. Contrast Media and Molecular Imaging, 2017, 2017, 1-5.	0.8	21
35	Extracting Cross-Sectional Clinical Images Based on Their Principal Axes of Inertia. Scanning, 2017, 2017, 1-8.	1.5	13
36	The brain effects of laser acupuncture at thirteen ghost acupoints in healthy individuals: A resting-state functional MRI investigation. Computerized Medical Imaging and Graphics, 2016, 54, 48-54.	5.8	11

LIANG-PING LUO

#	Article	IF	CITATIONS
37	Differential diagnosis of prostate cancer and noncancerous tissue in the peripheral zone and central gland using the quantitative parameters of DCE-MRI. Medicine (United States), 2016, 95, e5715.	1.0	12
38	CEST theranostics: label-free MR imaging of anticancer drugs. Oncotarget, 2016, 7, 6369-6378.	1.8	49
39	Clinical simulation training improves the clinical performance of Chinese medical students. Medical Education Online, 2015, 20, 28796.	2.6	23
40	Acoustic Radiation Force Impulse Elastography for Efficacy Evaluation after Hepatocellular Carcinoma Radiofrequency Ablation: A Comparative Study with Contrast-Enhanced Ultrasound. BioMed Research International, 2014, 2014, 1-7.	1.9	13
41	Tumor Volumes Measured From Static and Dynamic 18F-fluoro-2-deoxy-D-glucose Positron Emission Tomography-Computed Tomography Scan. Journal of Computer Assisted Tomography, 2014, 38, 209-215.	0.9	7
42	Size of solitary pulmonary nodule was the risk factor of malignancy. Journal of Thoracic Disease, 2014, 6, 668-76.	1.4	16
43	Role of the texture features of images in the diagnosis of solitary pulmonary nodules in different sizes. Chinese Journal of Cancer Research: Official Journal of China Anti-Cancer Association, Beijing Institute for Cancer Research, 2014, 26, 451-8.	2.2	13
44	Differentiation of Central Lung Cancer from Atelectasis: Comparison of Diffusion-Weighted MRI with PET/CT. PLoS ONE, 2013, 8, e60279.	2.5	42
45	Posttraumatic pulmonary pseudocyst. Journal of Trauma and Acute Care Surgery, 2012, 73, 1225-1228.	2.1	20
46	Ultrasound- and Liposome Microbubble-Mediated Targeted Gene Transfer to Cardiomyocytes In Vivo Accompanied by Polyethylenimine. Journal of Ultrasound in Medicine, 2011, 30, 1247-1258.	1.7	27
47	Fractal description and clinical controlled study of infants' cerebral medical computed tomography. , 2010, , .		0
48	MRI and CT in the Differential Diagnosis of Pleural Disease. Chest, 2000, 118, 604-609.	0.8	142